J. Fluid Mech. (2022), *vol*. 950, A14, doi:10.1017/jfm.2022.809

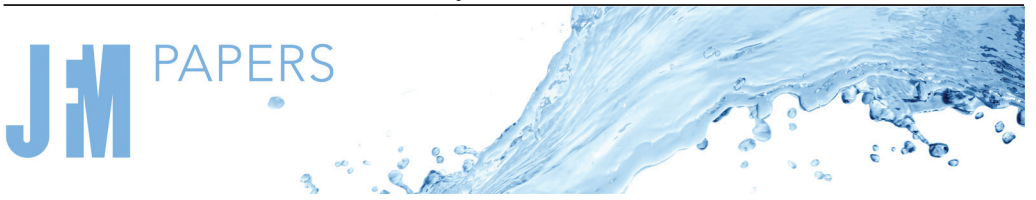

The Mott-Smith solution to the regular shock reflection problem

M.Yu. Timokhin[1,2,3,†], A.N. Kudryavtsev[2] and Ye.A. Bondar[2]

[1]Lomonosov Moscow State University, 119991 Moscow, Russia

[2]Khristianovich Institute of Theoretical and Applied Mechanics, 630090 Novosibirsk, Russia

[3]Moscow Aviation Institute, 125993 Moscow, Russia

(Received 15 April 2022; revised 2 August 2022; accepted 2 September 2022)

The classical Mott-Smith solution for one-dimensional normal shock wave structure is extended to the two-dimensional regular shock reflection problem. The solution for the non-equilibrium molecular velocity distribution function along the symmetry-plane streamline is obtained as a weighted sum of four Maxwellians. An analysis of applicability of the solution has been performed using the results of direct simulation Monte Carlo calculations for a range of incident shock wave intensities. Accuracy of the solution improves with increasing Ma_n, the Mach number normal to the shock front, so that the solution becomes rather accurate for strong shocks with $Ma_n > 8$.

Key words: shock waves, kinetic theory, gas dynamics

1. Introduction

In the course of many years of research on normal shock wave internal structure, it has become a benchmark problem for testing new mathematical models of rarefied and non-equilibrium flows (Pham-Van-Diep, Erwin & Muntz 1991; Ohwada 1993; Torrilhon & Struchtrup 2004; Kudryavtsev, Shershnev & Ivanov 2008; Johnson 2013; Timokhin *et al.* 2016; Velasco & Uribe 2019; Shoev, Timokhin & Bondar 2020; Jadhav, Gavasane & Agrawal 2021). It has been caused by the importance of shock-wave phenomena in real-life applications, simplicity of the mathematical formulation and availability of experimental data (Hansen & Hornig 1960; Schmidt 1969; Alsmeyer 1976; Pham-Van-Diep, Erwin & Muntz 1989; Timokhin *et al.* 2020).

The bimodal Mott-Smith (M-S) solution (Mott-Smith 1951; Tamm 1965) is a classical solution of this fundamental problem. The solution of the Boltzmann equation is based on the approximation of the non-equilibrium molecular velocity distribution in the form

† Email address for correspondence: timokhin@physics.msu.ru

of the sum of two Maxwellians with unknown weight coefficients. The Maxwellians correspond to two equilibrium states of the gas on opposite sides of the shock wave. The bimodal character of the distribution function becomes more evident with the increase of shock wave Mach number. It leads to the fact that this analytical solution is more applicable for prediction of the phase density for strong shock waves (e.g. Kogan 1969; Bird 1967; Pham-Van-Diep *et al.* 1989; Xu & Huang 2010; Timokhin & Rukhmakov 2021). Further investigation of the shock wave structure showed that the M-S solution does not allow reproduction of such non-equilibrium effects as temperature overshoot (e.g. Holway 1965*b*; Erofeev & Friedlander 2002; Ivanov *et al.* 2012; Timokhin *et al.* 2015). Mott-Smith's original approach was later modified by using different basis functions (Muckenfuss 1962; Holway 1965*a*; Kogan 1969; Solovchuk & Sheu 2010), or the introduction of the third basis function (Salwen, Grosch & Ziering 1964). These modifications made the M-S approximation much closer to the Boltzmann equation solution for a wide range of Mach numbers (e.g. Solovchuk & Sheu 2010, 2011).

Despite the existing disadvantages of the original M-S solution in the quantitative description of the structure of a one-dimensional (1-D) shock wave, this solution provides excellent qualitative description of the transition of a gas from one equilibrium state to the other across the shock at the level of molecular velocity distributions.

2. Problem formulation and mathematical model

Real supersonic flows are rarely 1-D. Among steady two-dimensional (2-D) flows, there are some examples that retain important features of the 1-D normal shock wave problem. Probably the simplest example is the problem of stationary regular reflection of an oblique shock wave from the plane of symmetry (e.g. Ben-Dor 2007; Xue *et al.* 2020). Such a flow is illustrated by a numerical density flow field as shown in figure 1. The direction of the supersonic flow (region 1) is from left to right. The flow is deflected in the oblique incident shocks (IS) and returns to its original direction passing through the reflected shocks (RS). The angles of incident and reflected oblique shock waves are denoted in figure 1 as α and β, respectively. It should be noted that the inviscid solution of this problem consists of four zones of a uniform supersonic flow divided by discontinuities (in contrast with two uniform flow regions divided by one discontinuity in the 1-D shock case). This solution can be determined analytically if one knows the incoming flow Mach number and the IS angle α (Ben-Dor 2007). Similarly, in the inviscid 1-D normal shock problem the analytical solution consists of two zones of uniform flow divided by one discontinuity and is fully determined by the shock Mach number. In this regard, the regular reflection problem can be considered as an extension of the normal shock structure problem to a more complicated 2-D case. If viscosity and heat conduction are taken into account, the shock waves acquire their internal structure, and in the vicinity of the reflection point (the origin in figure 1) the flow becomes essentially 2-D (Ivanov *et al.* 2002; Khotyanovsky *et al.* 2009; Bondar *et al.* 2019; Shoev & Ogawa 2019). It leads to the appearance of the so-called non-Rankine–Hugoniot zone (Sternberg 1959; Khotyanovsky *et al.* 2009; Ivanov *et al.* 2010). No analytical solution is known for the viscous flow in the vicinity of the reflection point, however, in the far field the 1-D analytical M-S solution is valid for oblique shocks in the direction normal to it. The presence of several equilibrium regions and non-equilibrium transitions between them leads to the idea of a qualitative M-S description of the flow in the vicinity of the reflection point. As it will be shown below, it is possible to obtain a solution to this 2-D problem along the symmetry plane. The goal of the present work is to obtain this solution for the gas of Maxwell molecules

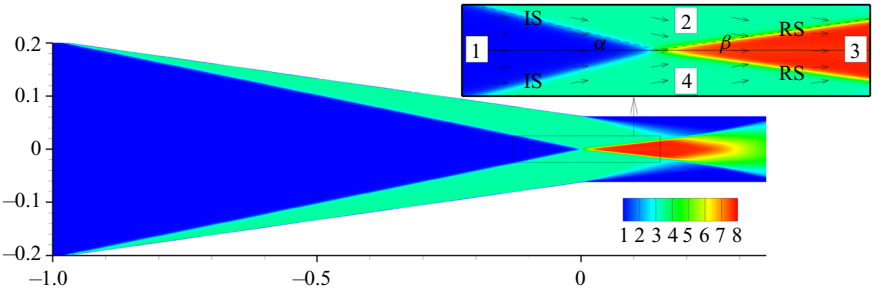

Figure 1. Density flow field for $Ma_n = 4.0$.

(similarly to the original M-S solution) and to analyse its accuracy by comparison with the direct simulation Monte Carlo (DSMC) numerical results.

The Boltzmann equation for a monatomic gas stationary 2-D flow in the absence of external forces can be written as follows:

$$v_x \frac{\partial f}{\partial x} + v_y \frac{\partial f}{\partial y} = J, \tag{2.1}$$

where $f(x, y, \boldsymbol{v})$ is a molecular velocity distribution function, $\boldsymbol{v}(v_x, v_y, v_z)$ is the vector of molecular velocity and J is the collision integral. We assume the solution of (2.1) can be approximated by a four-term sum,

$$f(x, y, \boldsymbol{v}) = \sum_{i=1}^{4} n_i(x, y) f_i(v_x, v_y, v_z), \tag{2.2}$$

where the $f_i(v_x, v_y, v_z)$ functions represent the Maxwellian velocity distributions of four equilibrium regions of the flow (see figure 1),

$$f_i(\boldsymbol{v}) = \left(\frac{1}{2\pi\theta_i}\right)^{3/2} \exp\left[-\frac{(v_x - U_i)^2 + (v_y - V_i)^2 + v_z^2}{2\theta_i}\right], \tag{2.3}$$

where $\theta_i = kT_i/m$. Here k and m are the Boltzmann constant and molecular mass, respectively; T_i, U_i and V_i are the values of gas temperature, x- and y-components of flow velocity in ith equilibrium region of the problem (see figure 1). Multiplying both sides of (2.1) by $\varphi(\boldsymbol{v})$ and integrating over the velocity space, one obtains the general transport equation of the attribute φ:

$$\frac{\partial}{\partial x}\int v_x \varphi f(x, y, \boldsymbol{v})\,\mathrm{d}\boldsymbol{v} + \frac{\partial}{\partial y}\int v_y \varphi f(x, y, \boldsymbol{v})\,\mathrm{d}\boldsymbol{v} = \int \varphi J\,\mathrm{d}\boldsymbol{v}. \tag{2.4}$$

Using the approximation (2.2) of $f(x, y, \boldsymbol{v})$, (2.4) can be written as follows:

$$\sum_{i=1}^{4}\left[n_{i_x}' \int v_x \varphi f_i(\boldsymbol{v})\,\mathrm{d}\boldsymbol{v} + n_{i_y}' \int v_y \varphi f_i(\boldsymbol{v})\,\mathrm{d}\boldsymbol{v}\right] = I_\varphi, \tag{2.5}$$

where $n_{i_x}' = \partial n_i/\partial x$, $n_{i_y}' = \partial n_i/\partial y$ and $I_\varphi = \int \varphi J\,\mathrm{d}\boldsymbol{v}$. The substitution of various attributes φ_k in (2.5) allows one to obtain a sufficient number of moment equations to find the spatial

functions $n_i(x, y)$. The right-hand side of the general transport equation (2.5) is equal to zero for the conserved quantities

$$\varphi_i = \left\{1, v_x, v_y, v_z, v^2\right\}, \quad i = \overline{1, 5}. \tag{2.6}$$

In the 2-D case the equation for $\varphi_4 = v_z$ vanishes due to the absence of momentum transfer in the z direction. If one writes down the conservation laws and higher moment equations along the symmetry plane streamline we can take into account the following conditions:

$$n_{2_x}' = n_{4_x}', \quad n_{2_y}' = -n_{4_y}', \quad n_{1_y}' = n_{3_y}' = 0. \tag{2.7a–c}$$

These conditions result in zeroing of the transport equation for $\varphi_3 = v_y$ on the plane of symmetry, which is explained by the absence of momentum transfer in the y direction. The remaining conservation laws can be written as follows:

$$U_1 n_{1_x}' + U_3 n_{3_x}' + 2U_2 n_{2_x}' + 2V_2 n_{2_y}' = 0, \tag{2.8}$$

$$(U_1^2 + c_1^2) n_{1_x}' + (U_3^2 + c_3^2) n_{3_x}' + 2(U_2^2 + c_2^2) n_{2_x}' + 2U_2 V_2 n_{2_y}' = 0, \tag{2.9}$$

$$U_1(U_1^2 + 5c_1^2) n_{1_x}' + U_3(U_3^2 + 5c_3^2) n_{3_x}' + 2(U_2^2 + V_2^2 + 5c_2^2)(U_2 n_{2_x}' + V_2 n_{2_y}') = 0, \tag{2.10}$$

where $c_i = \sqrt{\theta_i}$. To obtain the moment equations for the remaining attributes φ_k (for $k > 5$), it is necessary to know the value of the corresponding I_{φ_k}. Their values depend on the molecular interaction potential. The integrals of power functions φ_k can be expressed by the integrals of the Hermite polynomials (Kogan 1969). In the study, the moment equations were constructed for $\varphi_6 = v_x^2$, $\varphi_7 = v_y^2$, $\varphi_8 = v^2 v_x$, and $\varphi_9 = v_x^3$. The right-hand side of the corresponding moment equations in I_H notation can be written as

$$I_{v_x^2} = \theta I_{H_{xx}^{(2)}}, \quad I_{v_y^2} = \theta I_{H_{yy}^{(2)}}, \tag{2.11a,b}$$

$$I_{v^2 v_x} = \theta^{3/2}\left(I_{H_{xxx}^{(3)}} + I_{H_{xyy}^{(3)}} + I_{H_{xzz}^{(3)}}\right), \quad I_{v_x^3} = \theta^{3/2} I_{H_{xxx}^{(3)}} + \theta U I_{H_{xx}^{(2)}}. \tag{2.12a,b}$$

For the Maxwell molecules the values of I_H are known (Grad 1949; Kogan 1969). In the case of the second degree of the Hermite polynomials $H_{ij}^{(2)}$, the corresponding I_H is

$$I_{H_{ij}^{(2)}} = -6\gamma n^2 \frac{p_{ij}}{p}, \quad \gamma = A\sqrt{\frac{8K}{m}}, \tag{2.13a,b}$$

where K is the constant in the Maxwell molecular potential K/r^4, and $A = 0.343$ (e.g. Kogan 1969). Here $n = \sum_{i=1}^{4} n_i$ and p are number density and pressure, and $p_{ij} = m\int(C_i C_j - \frac{1}{3}C^2\delta_{ij}) f \, \mathrm{d}\boldsymbol{v}$, where C is the peculiar velocity of the molecules and δ_{ij} is the Kronecker delta. In the case of the third degree of the Hermite polynomials, the corresponding I_H is written as follows:

$$I_{H_{ijk}^{(3)}} = -\gamma n^2\left(9a_{ijk}^{(3)} - a_{ill}^{(3)}\delta_{jk} - a_{jll}^{(3)}\delta_{ik} - a_{kll}^{(3)}\delta_{ij}\right), \tag{2.14}$$

where the coefficients $a_{ijk}^{(3)}$ can be expressed via the components of heat flux vector $\boldsymbol{q}$ (see Kogan 1969),

$$a_{ijk}^{(3)} = \frac{2}{5}\frac{1}{p\sqrt{\theta}}\left(q_i\delta_{jk} + q_j\delta_{ik} + q_k\delta_{ij}\right), \tag{2.15}$$

where $q_i = (m/2)\int C^2 C_i f \mathrm{d}\boldsymbol{v}$. Then the remaining moment equations are given in the following form:

$$U_1(U_1^2 + 3c_1^2)n_{1_x}' + 2U_2(U_2^2 + 3c_2^2)n_{2_x}' + U_3(U_3^2 + 3c_3^2)n_{3_x}' + 2V_2(U_2^2 + c_2^2)n_{2_y}' = -6\gamma\frac{n}{m}p_{xx}, \tag{2.16}$$

$$U_1 c_1^2 n_{1_x}' + 2U_2(V_2^2 + c_2^2)n_{2_x}' + U_3 c_3^2 n_{3_x}' + 2V_2(U_2^2 + 3c_2^2)n_{2_y}' = -6\gamma\frac{n}{m}p_{yy}, \tag{2.17}$$

$$(U_1^4 + 8c_1^2U_1^2 + 5c_1^4)n_{1_x}' + (U_2^4 + V_2^2(U_2^2 + c_2^2) + 8c_2^2U_2^2 + 5c_2^4)n_{2_x}' + (U_3^4 + 8c_3^2U_3^2 + 5c_3^4)n_{3_x}' + 2U_2V_2(U_2^2 + V_2^2 + 7c_2^2)n_{2_y}' = -8\gamma\frac{n}{m}q_x, \tag{2.18}$$

$$(U_1^4 + 6c_1^2U_1^2 + 3c_1^4)n_{1_x}' + (U_2^4 + 6c_2^2U_2^2 + 3c_2^4)n_{2_x}' + (U_3^4 + 6c_3^2U_3^2 + 3c_3^4)n_{3_x}' + 2U_2V_2(U_2^2 + 3c_2^2)n_{2_y}' = -\frac{6}{5}\gamma\frac{n}{m}\left(4q_x + 15Up_{xx}\right), \tag{2.19}$$

where gas number density n and x-component of flow velocity U in the right-hand sides can be written as

$$n = n_1 + n_3 + 2n_2, \quad U = \left(n_1U_1 + n_3U_3 + 2n_2U_2\right)/n. \tag{2.20a,b}$$

The tensor components p_{xx}, p_{yy} and the heat flux component q_x can be represented as functions of n_1, n_2 and n_3 using (2.2):

$$p_{xx} = [4n_2n_3(U_2 - U_3)^2 - 2n_2(n_3 + 2n_2)V_2^2 + 2n_1(n_3(U_1 - U_3)^2 + 2n_2(U_1 - U_2)^2 - n_2V_2^2)]/(3n), \tag{2.21}$$

$$p_{yy} = -[n_1n_3(U_1 - U_3)^2 + 2n_2n_3(U_2 - U_3)^2 - 4n_2(n_3 + 2n_2)V_2^2 + 2n_1n_2((U_1 - U_2)^2 - 2V_2^2)]/(3n), \tag{2.22}$$

$$q_x = -[n_1(5c_1^2 + (U - U_1)^2)(U - U_1) + n_3(5c_3^2 + (U - U_3)^2)(U - U_3) + 2n_2(U - U_2)(5c_2^2 + (U - U_2)^2 + V_2^2)]/2. \tag{2.23}$$

The relations (2.16)–(2.19) are partial differential equations, where the left-hand sides contain the derivatives of concentrations with constant coefficients, and the right-hand sides contain functions of n_1, n_2 and n_3. All variables in the obtained equations can be non-dimensionalized with the free stream parameters (region 1 in figure 1)

$$\left.\begin{gathered} N_i = \frac{n_i}{n_{10}}, \quad N = \sum_{i=1}^{4} N_i, \quad \hat{U}_i = \frac{U_i}{c_1}, \quad \hat{V}_i = \frac{V_i}{c_1}, \quad \hat{c}_i = \frac{c_i}{c_1}, \\ \hat{\theta} = \frac{\theta}{c_1^2}, \quad \hat{p}_{ij} = \frac{p_{ij}}{mn_{10}c_1^2}, \quad \hat{q}_i = \frac{q_i}{mn_{10}c_1^3}, \quad \hat{x} = \frac{x}{\lambda_0}, \quad \hat{y} = \frac{y}{\lambda_0}, \end{gathered}\right\} \tag{2.24}$$

where n_{10} is the number density in equilibrium region 1 and $\lambda_0 = \frac{2}{15}(c_1/An_{10})\sqrt{m/\pi K}$ is the Maxwell molecule mean free path (Kogan 1969) in the free stream (see figure 1). Further analyses and presentation of the results will be carried out in dimensionless form.

It should be noted that these equations were obtained for the symmetry plane (for $y = 0$). The conditions for the symmetry plane lead to the fact that the only derivative with respect to the y-coordinate in these equations is n_{2y}'. It can be easily shown using (2.8). This derivative can be considered as a function of the x-coordinate at $y = 0$. The substitution of n_{2y}' with its expression from (2.8) leads to the following non-dimensionalized form of (2.9):

$$(\hat{U}_1^2 + \hat{c}_1^2 - \hat{U}_1\hat{U}_2)N_{1\hat{x}}' + (\hat{U}_3^2 + \hat{c}_3^2 - \hat{U}_2\hat{U}_3)N_{3\hat{x}}' + 2\hat{c}_2^2 N_{2\hat{x}}' = 0. \tag{2.25}$$

The solution (2.2) must satisfy the boundary conditions on the symmetry plane,

$$f(x \to -\infty, y = 0, \boldsymbol{v}) = n_{10} f_1(\boldsymbol{v}), \quad f(x \to +\infty, y = 0, \boldsymbol{v}) = n_{30} f_3(\boldsymbol{v}), \tag{2.26a,b}$$

where n_{30} is the number density in equilibrium region 3, respectively. These relations lead to the boundary conditions for N_1, N_2 and N_3:

$$N_1(-\infty) = N_{10}, \quad N_3(+\infty) = N_{30}, \quad N_1(+\infty) = N_2(\pm\infty) = N_3(-\infty) = 0. \tag{2.27a–c}$$

Integration of (2.25) taking into account conditions (2.27*a–c*) allows us to obtain the relation for N_1, N_2 and N_3 functions on the symmetry plane

$$N_1 = 1 + \frac{(\hat{U}_2\hat{U}_3 - \hat{U}_3^2 - \hat{c}_3^2)N_3 - 2\hat{c}_2^2 N_2}{\hat{U}_1^2 + \hat{c}_1^2 - \hat{U}_1\hat{U}_2}. \tag{2.28}$$

The resulting (2.28) with the rest of the moment equations (2.10), (2.16)–(2.19) and boundary conditions (2.27*a–c*) form an overdetermined system of equations for three required functions N_1, N_2 and N_3. An exact solution to the Boltzmann equation will satisfy any number of moment equations. In order to estimate the quality of the approximation, it is possible to obtain several solutions with the same approximating function, but with a different choice of moment equations (e.g. see Mott-Smith 1951; Salwen *et al.* 1964). In the present study we tested three sets of equations: (2.28) was supplemented by three various extra pairs of moment equations. The pairs were taken for the transport equations of following φ-attributes: $(v_x^2, v^2 v_x)$; $(v_y^2, v^2 v_x)$; (v_y^2, v_x^3). The relation (2.28) allows us to obtain the system of two differential equations for each φ-pair with respect to the functions $N_2(x)$ and $N_3(x)$ with two conditions $N_2(-\infty) = 0$ and $N_3(-\infty) = 0$ (see (2.27*a–c*)). Further, each pair of equations can be solved numerically similarly to the scheme described in Salwen *et al.* (1964).

3. Results and discussion

To observe the regular reflection of the incident oblique shock wave, the IS angle must be in the range $\alpha_M < \alpha < \alpha_D$. The Mach angle $\alpha_M = \arcsin(1/Ma_1)$ corresponds to the shock wave of zero intensity. The detachment angle α_D is the maximum angle at which, in accordance with the inviscid shock wave theory, the flow deflected in the oblique incident shock wave, IS, can return to its original direction passing through the reflected shock wave, RS (Ben-Dor 2007). Thus, the regular reflection is impossible above the detachment angle α_D so that, in experiments, irregular shock wave configurations consisting of more than two shock waves are observed instead (Hornung 1986). In the study, a sufficiently high free stream Mach number ($Ma_1 = 20$) was chosen to obtain a wide range of incident shock wave intensities (IS angles). In this case the Mach and detachment angles are $\alpha_M \approx 2.87^\circ$ and $\alpha_D \approx 35.36^\circ$, respectively. Figure 2(*a*) presents the solutions along the plane of symmetry for the example case $Ma_n = 8.0$ of three investigated pairs of equations.

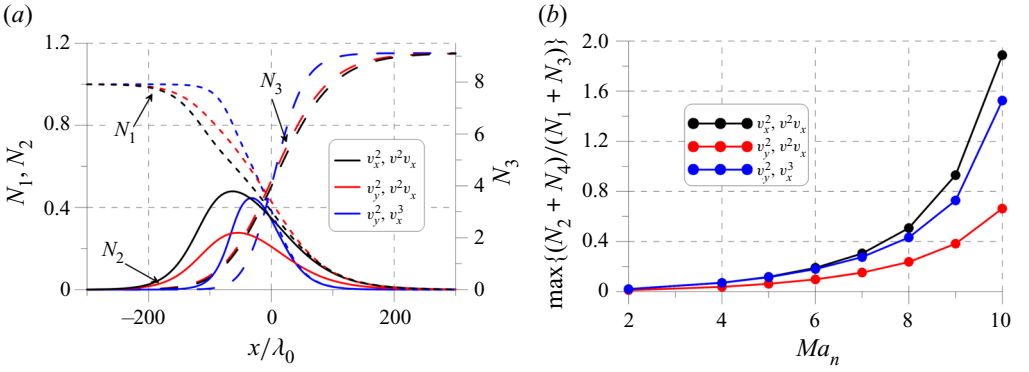

Figure 2. (*a*) The N_1, N_2 and N_3 distributions for $Ma_n = 8.0$ with different pairs of equations; (*b*) the $(N_2 + N_4)/(N_1 + N_3)$ maximum value dependence on the normal Mach number.

The origin here and in what follows corresponds to the point where $N(0) = (N_{10} + N_{30})/2$. These distributions of N_i functions are typical of the entire range of considered IS angles. As can be seen from the presented result, the studied pairs allow us to obtain qualitatively identical distributions of N_1, $N_2 = (N_2 + N_4)/2$ and N_3. The quantitative difference is primarily in the thickness of the transition region from state 1 to state 3, as well as in the magnitude of the maximum for N_2.

The contribution of N_2 and N_4 functions to the solution along the symmetry plane streamline to some extent demonstrates the effect of two-dimensionality of the flow on the solution. At a constant free stream Mach number this effect should increase with an increase of the IS angle and hence also the incident shock intensity. The maximum values of $(N_2 + N_4)/(N_1 + N_3)$ along the symmetry plane streamline can be considered as a measure of the mentioned contribution to the solution. The dependence of this parameter on the normal Mach number which governs the IS intensity is shown in figure 2(*b*). The contribution of the flow parts behind the incident shock to the symmetry plane solution increases with Ma_n for all types of the solution. While for $Ma_n < 4$ it can be considered insignificant, at normal Mach numbers as high as 10 this parameter can even exceed unity, which means at some points on the symmetry plane the contribution of regions 2 and 4 to the solution is even greater than that of the upstream and downstream regions 1 and 3. To analyse the applicability of the considered approach to the description of the density profile and molecular distribution function, benchmark numerical solutions to the considered problem were obtained by the DSMC method (Bird 1994). The 2-D computations were performed with the SMILE code (Ivanov *et al.* 2006) for $Ma_1 = 20$ and three values of $Ma_n = 4$, 8 and 10. On the one hand these values are relatively high so the multi-Maxwellian M-S solution could make sense, and on the other hand they represent three degrees of contribution of regions of 2 and 4 to the symmetry plane solution discussed above: negligible, moderate and high, respectively. The model of pseudo-Maxwell molecules was used in the computations which provide similar viscosity–temperature dependence as the Maxwell molecules but with more simple isotropic scattering (variable hard sphere (Bird 1994) model with the viscosity-temperature exponent equal to unity). The incident shock waves were generated by two wedges symmetrically placed in the supersonic flow. The density flow field for $Ma_n = 4$ is shown in figure 1. The wedges are used only for generation of oblique shocks and this is why the specular reflection condition was set on all the walls (which is a kinetic analogue of continuum impermeability conditions). The Knudsen number based on the length of the

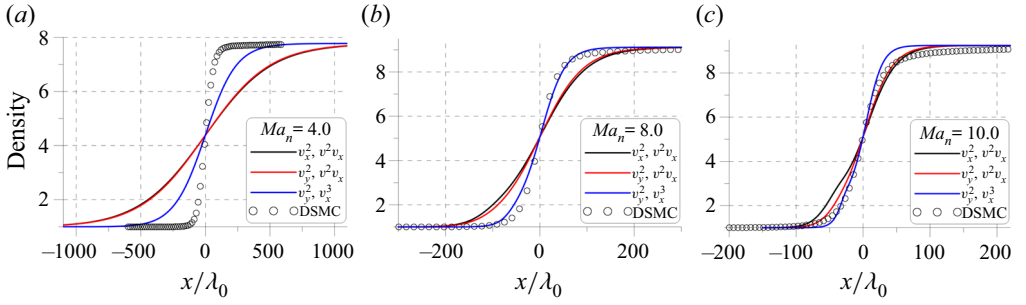

Figure 3. Density profiles for (*a*) $Ma_n = 4.0$, (*b*) $Ma_n = 8.0$ and (*c*) $Ma_n = 10.0$.

windward side of the wedge and the free stream mean free path was equal to 0.0005. Such a small Knudsen number allows the zone of interest where the regular reflection occurs to be unaffected by the expansion fans clearly visible in figure 1. The wedge angle was equal to 8.07°, 17.06° and 21.54° degrees and the gap between the trailing edges of the two wedges normalized to the length of the windward side of the wedge was equal to 0.124, 0.138 and 0.171 for Ma_n values of 4, 8 and 10, respectively. All the computational parameters satisfied the requirements for accurate DSMC modelling (Bird 1994): time step was small in comparison with mean collision time and cell residence time; and cells of the adaptive collisional grid were significantly smaller than local mean free path. The number of simulated particles in a virtual square cell with sides equal to the local mean free path was higher than 10 in the whole flow field which ensures the high accuracy of the solution (Shevyrin, Bondar & Ivanov 2005). Up to 80×10^6 simulated particles were used in a typical computation. A comparison of the density profiles along the plane of symmetry obtained using the M-S approximation with the DSMC results is shown in figure 3. At relatively low normal Mach numbers Ma_n (low intensity) of the incident shock wave, the thickness of the reflection region is greatly overestimated. This fact is demonstrated in figure 3(*a*) for $Ma_n = 4.0$. As the intensity of the incident shock wave decreases, the discrepancy between the M-S solution and the DSMC results only grows (such a comparison has been made but not presented in the paper). With the increase in the normal Mach number the M-S solution approaches the benchmark solution (see figure 3*b*,*c*). At the same time, the M-S solutions for various φ-pairs of equations become closer to each other. One can argue that the approximation function (2.2) approaches the solution of the Boltzmann equation with increasing Ma_n. This fact is explained by the strengthening of the modal nature of the distribution function which leads to better applicability of the M-S approximation for stronger shocks. Note that the solution for the φ-attributes $(v_y^2,\ v_x^3)$ predicts the DSMC density in the considered Mach number range better than the other two solutions. It has been demonstrated that the M-S density profiles approach the DSMC solution with increasing intensity of the incident shock wave. It should be noted that density is the most easily reproducible fluid flow macroparameter. Therefore, for more detailed analyses other flow macroparameters should be considered, which represent higher-order moments of the molecular distribution function.

Second-order moments which can be conveniently used for assessing the degree of thermal non-equilibrium are temperatures associated with various molecular thermal velocity components (Yen 1966)

$$\theta_j = \frac{kT_j}{m} = \frac{1}{n}\int C_j^2 f \,\mathrm{d}\boldsymbol{v}, \quad j = \{x, y, z\}, \quad \theta = \frac{1}{3}\left(\theta_x + \theta_y + \theta_z\right). \tag{3.1}$$

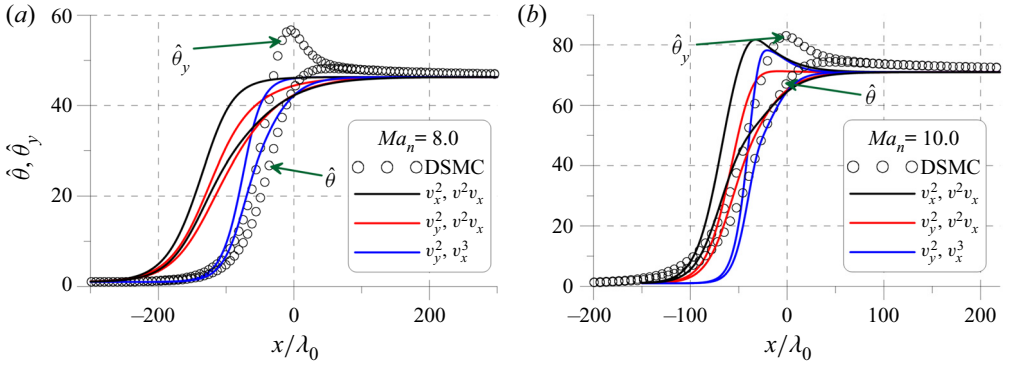

Figure 4. Total temperature and transverse temperature profiles for (*a*) $Ma_n = 8.0$ and (*b*) $Ma_n = 10.0$.

A well-known effect of strong thermal non-equilibrium in a normal shock wave is the presence of an overshoot in the longitudinal temperature θ_x at the back of the shock wavefront (Yen 1966). With an increase in the Mach number of the shock wave, an increase in the maximum in the longitudinal temperature also leads to the appearance of a maximum in the total temperature θ for Mach numbers $Ma > 3.9$ (Erofeev & Friedlander 2002). At the same time, the classical M-S solution for a normal shock wave does not provide the overshoot in the total temperature (Timokhin *et al.* 2015). In the considered 2-D flow, in contrast to the 1-D problem, in the vicinity of the regular reflection of oblique shock waves, an overshoot is observed in the transverse temperature θ_y. An overshoot of the total temperature is also clearly visible for all considered Mach numbers. Figure 4 shows the distributions of the transverse and total temperatures for $Ma_n = 8.0$ and $Ma_n = 10.0$. For $Ma_n = 4.0$ agreement between the M-S and DSMC results for higher-order moments is poor as it was observed for density and, therefore, these results are not presented. As can be seen, all considered solutions of the M-S approximation behave similarly to the density results (see figure 3). It is worth noting that at $Ma_n = 10.0$ the M-S approximation predicts the non-monotonic behaviour of the transverse temperature. On the other hand, as in the classical M-S solution for a 1-D shock wave, the distribution of the total temperature in a 2-D flow is a monotonic function along the symmetry plane. The figures 5 and 6 demonstrate a similar comparison of the distributions of the components of the stress tensor $\sigma_{ij} = p_{ij} - p\delta_{ij}$ (only diagonal components which are not equal to zero on the symmetry plane are presented) and the longitudinal component of the heat flux (which is the only non-zero component on the symmetry plane). All considered M-S solutions become closer to the benchmark DSMC solution in all considered flow parameters with increasing Ma_n. Better accuracy of the M-S solution for higher Ma_n can be explained by improvement in the quality of the M-S approximation (2.2) of the molecular distribution function with an increase in the intensity of the incident shock wave. As was demonstrated for density, the solution for the φ-attributes (v_y^2, v_x^3) agree with the benchmark DSMC results much better than two other solutions for all higher-order moments of the distribution function.

The proposed solution accuracy is further assessed by the comparison of the molecular velocity distribution with the DSMC results. The 1-D distribution functions depending only on x- or y-velocity components are considered. They are obtained from the three-dimensional distribution function by integration over two rest coordinates in the velocity space. The molecular velocity in all presented distributions is normalized to the

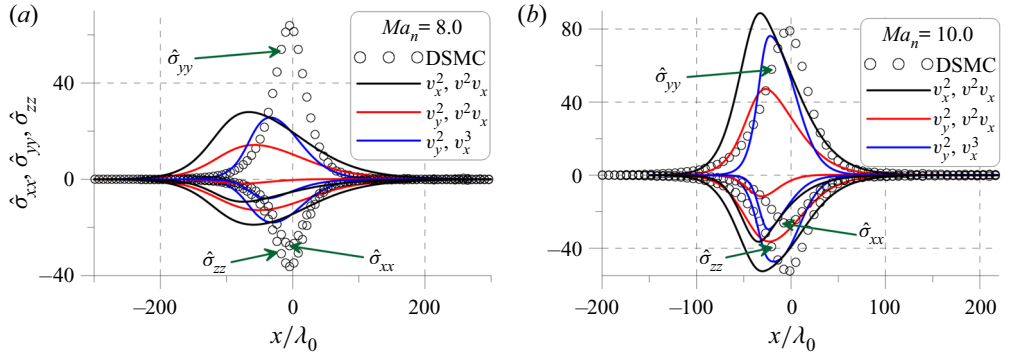

Figure 5. Stress tensor components for (*a*) $Ma_n = 8.0$ and (*b*) $Ma_n = 10.0$.

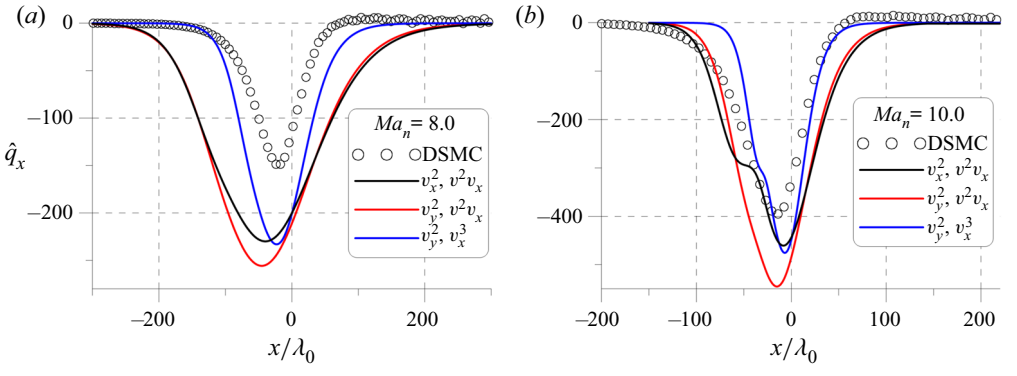

Figure 6. Heat flux for (*a*) $Ma_n = 8.0$ and (*b*) $Ma_n = 10.0$.

value of the most probable peculiar velocity $c_p = \sqrt{2}c_1$ in the free stream flow (region 1 in figure 1). Figures 7 and 8 present the results of comparison for local molecular velocity distribution functions for two values of normal Mach number. The M-S solution for the φ-attributes (v_y^2, v_x^3) is chosen for comparison because it is the most accurate variant of the solution in terms of predicting the DSMC macroparameters' profiles. The comparison was carried out at points on the symmetry plane with the same density values in the DSMC and the M-S solutions (two values close to those in regions 1 and 3 and two intermediate values). The presented results of the comparison demonstrate qualitatively correct descriptions of the flow transition from state 1 to state 3 by the M-S approach for all considered normal Mach numbers.

For each case, dashed lines mark the values of the most probable velocity components U_i and V_i for the modes of the corresponding solution (2.3). Let us consider the x-components of the velocities in more detail (see figures 7*a* and 8*a*). The value of U_1 for all the cases considered remains unchanged due to the constant value of the free stream Mach number. Changing of Ma_n results in varying the values of $U_2 = U_4$ and U_3. For the Mach number $Ma_n = 4.0$, the relative differences of U_2 and U_3 from U_1 are 2.8 % and 4.4 %, respectively. The basis modes of the solution in this case are very close to each other. At the same time, as Ma_n grows, these differences grow, which leads to an increase in the modality of the local solution. So, for $Ma_n = 10.0$ the same differences reach 18.6 % and 31.1 %, respectively. This explains the decrease in quantitative differences between the

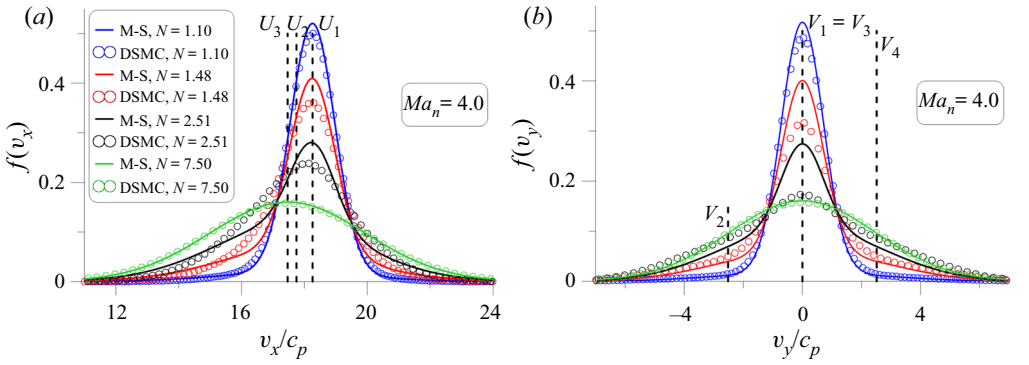

Figure 7. Velocity distribution functions $f(v_x)$ (*a*) and $f(v_y)$ (*b*) for $Ma_n = 4.0$.

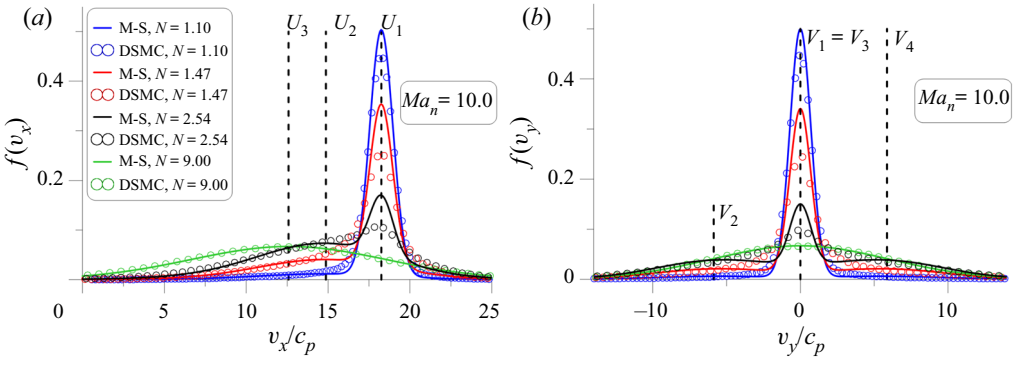

Figure 8. Velocity distribution functions $f(v_x)$ (*a*) and $f(v_y)$ (*b*) for $Ma_n = 10.0$.

DSMC and the M-S solutions. On the other hand, the modes in the DSMC distribution function turn out to be less pronounced for the intermediate values of density due to the presence of a large number of scattered molecules with velocities not representative of any Maxwellian mode. This strongly non-equilibrium effect is similarly observed in distribution functions inside normal shock waves (Pham-Van-Diep *et al.* 1989).

Strengthening of the modality of the velocity y-component distributions can also be observed (see figures 7*b* and 8*b*): the increase in the normal Mach number leads to increasing the difference of V_2 and V_4 from the zero values of V_1 and V_3. However, this effect is less pronounced. Some quantitative differences for the intermediate density values are also clearly observed for this velocity component.

4. Conclusion

As stated above, the classical M-S analytical solution provides a qualitative approximate kinetic description of the internal structure of a 1-D normal shock wave. The results obtained in the present study demonstrate the possibility of applying a similar approach to the 2-D problem of the regular reflection of shock waves. The analytical M-S approximation provides a clear qualitative description of the evolution of macroparameters and molecular distribution functions along the plane of symmetry in this 2-D strongly non-equilibrium flow. The accuracy of the solution becomes better with increasing intensity of the incident shock wave.

Funding. The work on development of the Mott-Smith solution was supported by the Russian Science Foundation (grant no. 20-71-00114). The DSMC computations and the analysis of the accuracy of the Mott-Smith solution were carried out within the state assignment of Ministry of Science and Higher Education of the Russian Federation (project no. 121030500143-6). Computational resources of the Equipment Sharing Center 'Mechanics' of ITAM SB RAS were employed for the DSMC computations.

Declaration of interests. The authors report no conflict of interest.

Author ORCIDs.
M.Yu. Timokhin https://orcid.org/0000-0001-8529-5300;
A.N. Kudryavtsev https://orcid.org/0000-0001-8119-5505;
Ye.A. Bondar https://orcid.org/0000-0002-9439-6573.

References

Alsmeyer, H. 1976 Density profiles in argon and nitrogen shock waves measured by the absorption of an electron beam. *J. Fluid Mech.* **74**, 497–513.

Ben-Dor, G. 2007 *Shock Wave Reflection Phenomena*. Springer.

Bird, G.A. 1994 *Molecular Gas Dynamics and the Direct Simulation of Gas Flows*. Clarendon Press.

Bird, G.A. 1967 The velocity distribution function within a shock wave. *J. Fluid Mech.* **30** (3), 479–487.

Bondar, Y., Shoev, G., Kokhanchik, A. & Timokhin, M. 2019 Nonequilibrium velocity distribution in steady regular shock-wave reflection. *AIP Conf. Proc.* **2132** (1), 120005.

Erofeev, A.I. & Friedlander, O.G. 2002 Momentum and energy transfer in a shock wave. *Fluid Dyn.* **379** (4), 614–623.

Grad, H. 1949 On the kinetic theory of rarefied gases. *Commun. Pure Appl. Maths* **2** (4), 331–407.

Hansen, K. & Hornig, D.F. 1960 Thickness of shock fronts in argon. *J. Chem. Phys.* **33** (3), 913–916.

Holway, L.H. 1965*a* Kinetic theory of shock structure using an ellipsoidal distribution function. In *Proceedings of the 4th International Symposium on Rarefied Gas Dynamics* (ed. J.H. Leeuw), vol. 1, pp. 193–215. Academic Press.

Holway, L.H. 1965*b* Temperature overshoots in shock waves. *Phys. Fluids* **8** (10), 1905–1906.

Hornung, H 1986 Regular and mach reflection of shock waves. *Annu. Rev. Fluid Mech.* **18** (1), 33–58.

Ivanov, I.E., Kryukov, I.A., Timokhin, M.Y., Bondar, Y.A., Kokhanchik, A.A. & Ivanov, M.S. 2012 Study of the shock wave structure by regularized Grad's set of equations. *AIP Conf. Proc.* **1501** (1), 215–222.

Ivanov, M., Bondar, Y., Khotyanovsky, D., Kudryavtsev, A. & Shoev, G. 2010 Viscosity effects on weak irregular reflection of shock waves in steady flow. *Prog. Aerosp. Sci.* **46** (2), 89–105.

Ivanov, M., Kashkovsky, A., Gimelshein, S., Markelov, G., Alexeenko, A., Bondar, Y., Zhukova, G., Nikiforov, S. & Vaschenkov, P. 2006 SMILE system for 2D/3D DSMC computations. In *Proceedings of 25th International Symposium on Rarefied Gas Dynamics*, pp. 21–28.

Ivanov, M.S., Ben-Dor, G., Elperin, T., Kudryavtsev, A.N. & Khotyanovsky, D.V. 2002 The reflection of asymmetric shock waves in steady flows: a numerical investigation. *J. Fluid Mech.* **469**, 71–87.

Jadhav, R.S., Gavasane, A. & Agrawal, A. 2021 Improved theory for shock waves using the OBurnett equations. *J. Fluid Mech.* **929**, A37.

Johnson, B.M. 2013 Analytical shock solutions at large and small Prandtl number. *J. Fluid Mech.* **726**, R4.

Khotyanovsky, D., Bondar, Y., Kudryavtsev, A., Shoev, G. & Ivanov, M.S. 2009 Viscous effects in steady reflection of strong shock waves. *AIAA J.* **47** (5), 1263–1269.

Kogan, M.N. 1969 *Rarefied Gas Dynamics*. Plenum.

Kudryavtsev, A.N., Shershnev, A.A. & Ivanov, M.S. 2008 Comparison of different kinetic and continuum models applied to the shock-wave structure problem. *AIP Conf. Proc.* **1084** (1), 507–512.

Mott-Smith, H.M. 1951 The solution of the Boltzmann equation for a shock wave. *Phys. Rev.* **82**, 885–892.

Muckenfuss, C. 1962 Some aspects of shock structure according to the bimodal model. *Phys. Fluids* **5** (11), 1325–1336.

Ohwada, T. 1993 Structure of normal shock waves: direct numerical analysis of the Boltzmann equation for hard-sphere molecules. *Phys. Fluids* A **5** (1), 217–234.

Pham-Van-Diep, G., Erwin, D. & Muntz, E.P. 1989 Nonequilibrium molecular motion in a hypersonic shock wave. *Science* **245** (4918), 624–626.

Pham-Van-Diep, G.C., Erwin, D.A. & Muntz, E.P. 1991 Testing continuum descriptions of low-mach-number shock structures. *J. Fluid Mech.* **232**, 403–413.

SALWEN, H., GROSCH, C.E. & ZIERING, S. 1964 Extension of the Mott-Smith method for a one-dimensional shock wave. *Phys. Fluids* **7** (2), 180–189.

SCHMIDT, B. 1969 Electron beam density measurements in shock waves in argon. *J. Fluid Mech.* **39** (2), 361–373.

SHEVYRIN, A.A., BONDAR, Y.A. & IVANOV, M.S. 2005 Analysis of repeated collisions in the DSMC method. In *Proceedings of 24th International Symposium on Rarefied Gas Dynamics* (ed. M. Capitelli), pp. 565–570. American Institute of Physics.

SHOEV, G. & OGAWA, H. 2019 Numerical study of viscous effects on centreline shock reflection in axisymmetric flow. *Phys. Fluids* **31** (2), 026105.

SHOEV, G.V., TIMOKHIN, M.Y. & BONDAR, Y.A. 2020 On the total enthalpy behavior inside a shock wave. *Phys. Fluids* **32** (4), 041703.

SOLOVCHUK, M.A. & SHEU, T.W.H. 2010 Prediction of shock structure using the bimodal distribution function. *Phys. Rev.* E **81**, 056314.

SOLOVCHUK, M.A. & SHEU, T.W.H. 2011 Prediction of strong-shock structure using the bimodal distribution function. *Phys. Rev.* E **83**, 026301.

STERNBERG, J. 1959 Triple-shock-wave intersections. *Phys. Fluids* **2** (2), 179–206.

TAMM, I.E. 1965 On the width of high-intensity shock waves [in Russian]. *Tr. Fiz. Inst. P. N. Lebedev Akad. Nauk SSSR* **99** (2), 231–241.

TIMOKHIN, M. & RUKHMAKOV, D. 2021 Local non-equilibrium phase density reconstruction with Grad and Chapman-Enskog methods. *J. Phys.: Conf. Ser.* **1959** (1), 012049.

TIMOKHIN, M.Y., BONDAR, Y.A., KOKHANCHIK, A.A., IVANOV, M.S., IVANOV, I.E. & KRYUKOV, I.A. 2015 Study of the shock wave structure by regularized Grad's set of equations. *Phys. Fluids* **27**, 037101.

TIMOKHIN, M.Y., STRUCHTRUP, H., KOKHANCHIK, A.A. & BONDAR, Y.A. 2016 The analysis of different variants of R13 equations applied to the shock-wave structure. *AIP Conf. Proc.* **1786**, 140006.

TIMOKHIN, M.Y., TIKHONOV, M., MURSENKOVA, I.V. & ZNAMENSKAYA, I.A. 2020 Shock-wave thickness influence to the light diffraction on a plane shock wave. *Phys. Fluids* **32** (11), 116103.

TORRILHON, M. & STRUCHTRUP, H. 2004 Regularized 13-moment equations: shock structure calculations and comparison to Burnett models. *J. Fluid Mech.* **513**, 171–198.

VELASCO, R.M. & URIBE, F.J. 2019 Shock-wave structure according to a linear irreversible thermodynamic model. *Phys. Rev.* E **99**, 023114.

XU, K. & HUANG, J.-C. 2010 A unified gas-kinetic scheme for continuum and rarefied flows. *J. Comput. Phys.* **229** (20), 7747–7764.

XUE, L., SCHRIJER, F.F.J., VAN OUDHEUSDEN, B.W., WANG, C., SHI, Z. & CHENG, K. 2020 Theoretical study on regular reflection of shock wave–boundary layer interactions. *J. Fluid Mech.* **899**, A30.

YEN, S.M. 1966 Temperature overshoot in shock waves. *Phys. Fluids* **9**, 1417–1418.